Applied Catalysis B: Environmental 142–143 (2013) 278–289

Contents lists available at SciVerse ScienceDirect

Applied Catalysis B: Environmental

journal homepage: www.elsevier.com/locate/apcatb

NOx-assisted soot combustion over dually substituted perovskite catalysts $La_{1-x}K_xCo_{1-y}Pd_yO_{3-\delta}$

Xin Guo [a], Ming Meng [a,*], Fangfang Dai [a], Qian Li [b], Zhaoliang Zhang [b,*], Zheng Jiang [c], Shuo Zhang [c], Yuying Huang [c]

[a] Tianjin Key Laboratory of Applied Catalysis Science & Engineering, School of Chemical Engineering & Technology, Tianjin University, Tianjin 300072, PR China
[b] Shandong Provincial Key Laboratory of Fluorine Chemistry and Chemical Materials, School of Chemistry and Chemical Engineering, University of Jinan, Jinan 250022, PR China
[c] Shanghai Synchrotron Radiation Facility, Shanghai Institute of Applied Physics, Chinese Academy of Sciences, Shanghai 201204, PR China

ARTICLE INFO

Article history:
Received 2 February 2013
Received in revised form 17 April 2013
Accepted 19 May 2013
Available online 25 May 2013

Keywords:
Soot combustion
Nitrogen oxides
Perovskite
Pd substitution
Mechanism

ABSTRACT

A series of dually substituted perovskite catalysts $La_{1-x}K_xCo_{1-y}Pd_yO_{3-\delta}$ ($x = 0$, 0.1; $y = 0$, 0.05) were successfully synthesized through a citrate-based sol–gel process, and employed for soot combustion in the presence of NOx. The physicochemical properties of them were systematically characterized by N_2-sorption, XRD, XPS, SEM, HRTEM, XANES, EXAFS, H_2-TPR, soot-TPR, FT-IR and TG/DTA. The activity evaluation results show that among all catalysts $La_{0.9}K_{0.1}Co_{0.95}Pd_{0.05}O_{3-\delta}$ possesses the highest performance, exhibiting the lowest T_i and T_m (219 °C and 360 °C), the narrowest temperature range ($T_f - T_i = 162$ °C) and the lowest activation energy (93.6 kJ/mol) for soot combustion. The catalyst $La_{0.9}K_{0.1}Co_{0.95}Pd_{0.05}O_{3-\delta}$ shows relatively larger BET surface area, smaller crystallite size and higher dispersion of Pd. Additionally, this catalyst also possesses the best reducibility and highest oxidibility as revealed by H_2-TPR and soot-TPR. The Pd ions with high valence (Pd^{3+}, Pd^{4+}) in distorted octahedral coordination environment as demonstrated by XPS, XANES and EXAFS are much more active for NO oxidation and soot combustion than the bivalent Pd ions with square-planar coordination symmetry. Based upon the characterization results and catalytic performance, a mechanism containing two reaction pathways namely direct soot oxidation by surface adsorbed oxygen species in oxygen vacancies and the NO_2-assisted soot oxidation is proposed.

1. Introduction

Rapid consumption of petroleum resources and remarkable increase of greenhouse emissions have brought us serious problems including energy shortage and environment pollutions. Both the improvement of energy usage efficiency and the elimination of pollutants are urgent missions to related scientists worldwide. Diesel engines operating at lean condition possess high fuel efficiency, high export power and excellent durability, so, they have been widely employed in many kinds of vehicles such as light and heavy trucks, steamships and even private cars [1]. However, the exhausts of diesel engines contain a lot of pollutants including unburned CO/hydrocarbons, solid-state soot particulates and nitrogen oxides (NOx). It is well known that the soot particulates with the size less than 2.5 μm can be easily breathed in the lungs by the animals, causing serious pulmonary diseases such as cancers. Therefore, it is highly necessary to eliminate the soot particulates before they are released to air. Nowadays, the catalytic combustion technique combined with diesel particulate filters (DPFs) is regarded as the most potential and efficient after-treatment technology for soot removal, in which soot is first trapped by DPFs and then removed via catalytic combustion on the catalysts coated on them [2,3]. Since the temperature of diesel exhaust usually falls in the range from 200 to 400 °C, the catalysts are required to possess particularly high activity so that they can match the temperature of the exhausts from diesel engines. Up to now, many kinds of catalysts have been investigated and employed to soot combustion; among them, supported noble metal catalysts and perovskite-type oxide catalysts exhibit very high activity for soot combustion. On noble metal catalysts, soot can be oxidized efficiently at relatively low temperatures, especially in NOx-containing atmospheres, because noble metals can oxidize NO to NO_2, a stronger oxidizer to soot oxidation as compared with O_2 and NO [4–6]. However, due to the limited resources, noble metal catalysts are very expensive than base metal catalysts, which restricts the extensive employment of noble metal catalysts. Although perovskite-based

* Corresponding authors. Tel.: +86 022 2789 2275; fax: +86 022 2789 2275.
E-mail address: mengm@tju.edu.cn (M. Meng).

0926-3373/$ – see front matter © 2013 Elsevier B.V. All rights reserved.
http://dx.doi.org/10.1016/j.apcatb.2013.05.036

catalysts often show relatively lower activity than noble metal catalysts for soot combustion, they still have attracted much attention owing to their much lower prices, good sulfur-resistance and high chemical/thermal/structural stability. In the reported perovskites, La-based perovskites are the most extensively studied ones, some of which exhibit excellent performance for soot combustion, giving an activity order of $LaCoO_3$ > $LaMnO_3$ > $LaFeO_3$ [7]. Through partial substitution of cations at A or/and B sites, the activity of perovskite-based catalysts can be further improved because of the generation of oxygen vacancies and/or the modification of the valence for A-, B-sites cations. In our previous work, we successfully performed simultaneous substitution of A- and/or B-sites cations by alkali metals such as K and transition metal elements such as Cu and Co, respectively; and we found that simultaneous substitution is a feasible and much more efficient way to increase the activity of perovskite-based catalysts in comparison with single substitution or non-substitution [8–10].

It is well known that the oxidation capability of perovskites mainly depends on the kinds of B-site cations. For improving the activity of perovskites, small amounts of noble metals such as Pt or Pd are often doped into the perovskite structures, especially the Pd, which has been widely used in three-way catalysts for automotive exhaust purification [11–14]. However, the simultaneous substitution of A- and B-sites cations in Pd-doped perovskites is seldom investigated, and no information about the structures and catalytic performance of such dually substituted perovskites is known. In addition, the supported noble metals (e.g. Pt, Pd) catalysts can readily sinter as used in relatively high-temperature oxidation reaction such as soot combustion, resulting in significant decrease of thermal stability and catalytic activity; so, exploration of new Pd-based catalysts is also necessary. For this consideration, in this work, a small amount of noble metal Pd was doped into $LaCoO_3$ perovskite to partially substitute the Co ions; meanwhile, the La ions at A-sites are also partially substituted by K to obtain a series of Pd-containing dually substituted perovskite catalysts ($La_{1-x}K_xCo_{0.95}Pd_{0.05}O_{3-\delta}$). For comparison, by using impregnation method conventional alumina supported catalyst Pd/Al_2O_3 and another series of supported Pd catalysts ($Pd/La_{1-x}K_xCoO_{3-\delta}$) are also prepared and investigated. The techniques of XRD, XPS, HRTEM, XANES and EXAFS have been employed to characterize the versatile structures of as-prepared catalysts including the bulk and surface structures, nanoscale morphology and lattice structures, coordination structures and chemical states of Pd species. The reducibility and surface oxygen species of the catalyst are studied by H_2-TPR and soot-TPR, respectively. It is found that the dually substituted perovskites do show remarkably improved catalytic activity for soot combustion. In view of the amount of active oxygen species and oxygen vacancies, reducibility, structures and chemical valences of Pd, the promotional effect of simultaneous substitution on the catalytic activity of the catalysts are discussed in detail; meanwhile, based upon the characterization results and catalytic performance, a likely mechanism for soot combustion over such dually substituted perovskites is proposed.

2. Experimental

2.1. Catalyst preparation

A series of nanometric perovskite catalysts $La_{1-x}K_xCo_{1-y}Pd_yO_{3-\delta}$ (x = 0, 0.1; y = 0, 0.05) were synthesized by a sol–gel process [15,16]. $La(NO_3)_3{\cdot}6H_2O$, $Co(NO_3)_2{\cdot}9H_2O$, KNO_3, $Pd(NO_3)_2{\cdot}2H_2O$ and citric acid (CA) (supplied by Tianjin Guangfu Fine Chemicals Research Institute) were used as precursor salts. The molar ratio of citric acid to the total metal ions is 1:1. During the preparation of $La_{1-x}K_xCo_{1-y}Pd_yO_{3-\delta}$, the required metal salts and citric acid were first dissolved together in deionized water and stirred for about 24 h at room temperature; then the formed solution was transferred into a vacuum rotary evaporator to remove the surplus water at 60 °C until a viscous liquid gel was obtained. In the next, the wet gel was dried homogenously in air flow at 120 °C overnight to obtain a dried precursor. After pre-calcination at 350 °C for 2 h to make the nitrates decompose, the precursor was further calcined at 700 °C for 4 h in air flow to form spongeous powder of final catalysts.

For another series of supported catalysts $Pd/La_{1-x}K_xCoO_{3-\delta}$ (x = 0, 0.1), the $La_{1-x}K_xCoO_{3-\delta}$ perovskites were first prepared as above; then an aqueous solution containing a desired amount of $Pd(NO_3)_2$ was impregnated on $La_{1-x}K_xCoO_{3-\delta}$. After drying at 80 °C for 12 h, the catalyst was calcined at 500 °C for 4 h in air flow. The palladium weight loading in both $La_{1-x}K_xCo_{1-x}Pd_xO_{3-\delta}$ and $Pd/La_{1-x}K_xCoO_{3-\delta}$ is about 2.1 wt.%. For convenience, the as-prepared catalysts of $LaCoO_3$, $La_{0.9}K_{0.1}CoO_{3-\delta}$, $LaCo_{0.95}Pd_{0.05}O_{3-\delta}$, $La_{0.9}K_{0.1}Co_{0.95}Pd_{0.05}O_{3-\delta}$, $Pd/LaCoO_3$ and $Pd/La_{0.9}K_{0.1}CoO_{3-\delta}$ are denoted as LC, LKC, LCP, LKCP, P/LC, P/LKC, respectively.

2.2. Catalyst characterization

X-ray diffraction (XRD) patterns were recorded on an X' pert Pro rotatory diffractometer (Rigaku Technologies Company) operating at 200 mA and 40 kV using Cu K_α as radiation source (λ = 0.15418 nm). The data of 2θ from 10° to 90° were collected with a step size of 0.02°.

Fourier transform infrared spectra (FT-IR) were recorded on a Thermo Nicolet Nexus spectrometer. KBr and 1/100 sample (weight ratio) were mixed and ground into fine powder so as to make into a wafer for measurement. During spectra collecting, the resolution of 2 cm^{-1} was adopted with the wavenumber changing from 400 to 4000 cm^{-1}.

The measurement of specific surface area (SSA) of the catalysts was conducted on a Quantachrome QuadraSorb SI instrument using nitrogen sorption method. The samples were pretreated in vacuum at 300 °C for 4 h before experiments. The SSA was calculated using BET equation.

The morphology of the catalysts was determined with a Hitachi S4800 field emission-scanning electron microscope (FE-SEM). Before experiments, the samples were coated with a thin gold layer to improve the electrical conductivity. High resolution transmission electron microscopy (HRTEM) images and the energy dispersive spectra (EDS) were obtained on a JEM-2100F system at an accelerating voltage of 200 kV.

H_2-TPR measurements were performed on the TP-5079 TPDRO setup (supplied by the Tianjin Xianquan Instrument Company) equipped with a thermal conductivity detector (TCD). 5 vol.% H_2 balanced by pure N_2 was used as reductant at a flow rate of 30 mL/min. The test was carried out from room temperature to 800 °C at a heating rate of 10 °C/min.

X-ray photoelectron spectra (XPS) measurements were performed on a PHI-1600 ESCA spectrometer using Mg K_α (1253.6 eV) as radiation source. The base pressure was about 5×10^{-8} Pa. The binding energies were calibrated using C 1s peak at 284.6 eV as standard and quoted with a precision of ±0.2 eV.

The measurements of X-ray absorption near-edge structure (XANES) and extended X-ray absorption fine structure (EXAFS) of Pd *K*-edge were carried out on the XAFS station of 14W1 beamline of Shanghai Synchrotron Radiation Facility operating at about 300 mA and 3.5 GeV. The reference samples PdO and Pd-foil with a purity of 99.99% were purchased from Kunming Institute of Precious Metals of China. All of the samples were measured in the form of fine powder (<200 mesh) which was coated on the Scotch Magic Tape (3M 811) without using any dilution materials. The X-ray absorption spectra of the Pd *K*-edge of reference PdO and

Pd foil were recorded in transmittance mode, while those of the prepared samples were recorded in fluorescence mode due to the low content of Pd. A Si (3 1 1) double-crystal monochromator was used to monochromatize the X-ray, and a partial detuning between the silicon crystals was performed to suppress the high harmonics content. The back-subtracted EXAFS function was converted into k space and weighted by k^3 in order to compensate for the diminishing amplitude due to the decay of the photoelectron wave. The Fourier transforming of the k^3-weighted EXAFS data was performed in the range of $k = 3.5–14\ Å^{-1}$ using a Hanning function window to get the radial distribution function (RDF).

2.3. Activity evaluation

The catalytic activity of the prepared catalysts for soot combustion was evaluated by TG/DTA technique using Printex-U purchased from Degussa as the model soot. The soot was mixed with the catalyst in a weight ratio of 1:15 in an agate mortar for 10 min to reach a tight contact. The mixture was then loaded in the sample chamber and heated from room temperature to 600 °C at a heating rate of 5 °C/min in the atmosphere containing 600 ppm NO, 10 vol.% O_2 and balance N_2 (flow rate: 100 mL/min). In this work, characteristic temperatures such as soot ignition temperature (denoted as T_i), soot maximal conversion temperature (denoted as T_m) and soot complete conversion temperature (denoted as T_f) were used to compare the catalytic activity of the catalysts. To study the influence of atmosphere, TG/DTA experiments were performed separately in several kinds of atmospheres including pure N_2, 600 ppm NO/N_2, 10 vol.% O_2/N_2, (600 ppm NO + 10 vol.% O_2)/N_2, 400 ppm NO_2/N_2, (400 ppm NO_2 + 10 vol.% O_2)/N_2.

The activation energy (E_a) for soot combustion over prepared catalysts was measured by TG/DTA technique, using the as-reported Ozawa method [17]. According to the Ozawa method, the activation energy can be calculated by the following equation:

$$\ln B = -0.4567\frac{E_a}{R}\frac{1}{T} + C$$

Here, C is a constant and B is the heating rate. In this work, soot combustion tests were carried out at three heating rates ($B_1 = 2$ °C/min, $B_2 = 5$ °C/min, $B_3 = 10$ °C/min). Then each pair of $\ln B$ and $1/T$ of these data were used for plotting. From the equation, E_a could be calculated by the slope of the plotted line.

3. Results and discussion

3.1. Catalyst characterization

3.1.1. XRD

Fig. 1 shows the XRD patterns of the catalysts $La_{1-x}K_xCo_{1-y}Pd_yO_{3-\delta}$ and $Pd/La_{1-x}K_xCoO_{3-\delta}$. From Fig. 1(a), it is seen that all the catalysts display typical diffraction peaks of $LaCoO_3$ perovskite (JPCDS 48-0123), demonstrating that the perovskite structures are well maintained after the partial substitution of La/Co by K/Pd or the direct impregnation of Pd. However, for the samples substituted by K (LKC, LKCP, P/LKC), several very weak diffraction peaks of Co_3O_4 appear, implying the existence of a small amount of Co_3O_4 in these samples; while for the sample only substituted by Pd (LCP) no trace of Co_3O_4 phase could be detected. Besides, among the samples substituted by K, the peak at $2\theta = 36.9°$ attributed to Co_3O_4 for the dually substituted catalyst (LKCP) is much weaker than other two samples LKC and P/LKC, revealing that the substitution of Co by Pd at B-site can inhibit the formation of Co_3O_4 and is favorable to perovskite structure. To confirm the penetration of K and/or Pd into the lattice of perovskite structure, the regional patterns containing the two strongest peaks ($2\theta = 32.8°$, 33.3°) of $LaCoO_3$ perovskite, as indicated by dotted lines in Fig. 1(a), are enlarged and displayed in Fig. 1(b). For the singly substituted samples (LKC, LCP), the diffraction peaks shift to lower 2θ position as compared with those for LC, suggesting the successful incorporation of K or Pd ions into the lattice of perovskite structure because the larger sizes of K^+ and Pd^{2+} than La^{3+} and Co^{3+} can expand the perovskite lattice. For the dually substituted sample (LKCP), the diffraction peaks further shift to lower 2θ position, implying that the simultaneous substitution of La^{3+} and Co^{3+} by K^+ and Pd^{2+} is successfully achieved. In order to provide more convictive evidence for Pd incorporation into the perovskite lattice, the XRD patterns of the catalysts with different amounts of Pd are shown in Fig. S1 and the Rietveld refinement of the data are given in Table S1. It is clearly seen that the two strongest peaks ($2\theta = 32.8°$, 33.3°) of $LaCoO_3$ perovskite shift to lower positions and the cell volumes of the catalysts also expand from 333.724 to 333.897 $Å^3$ with the increase of Pd due to the larger sizes of Pd^{2+} than Co^{3+}, which confirm the successful incorporation of Pd ions into the lattice of perovskite. On the contrary, no peak shifts are observed for the impregnated samples P/LC and P/LKC, as compared with the corresponding supports LC

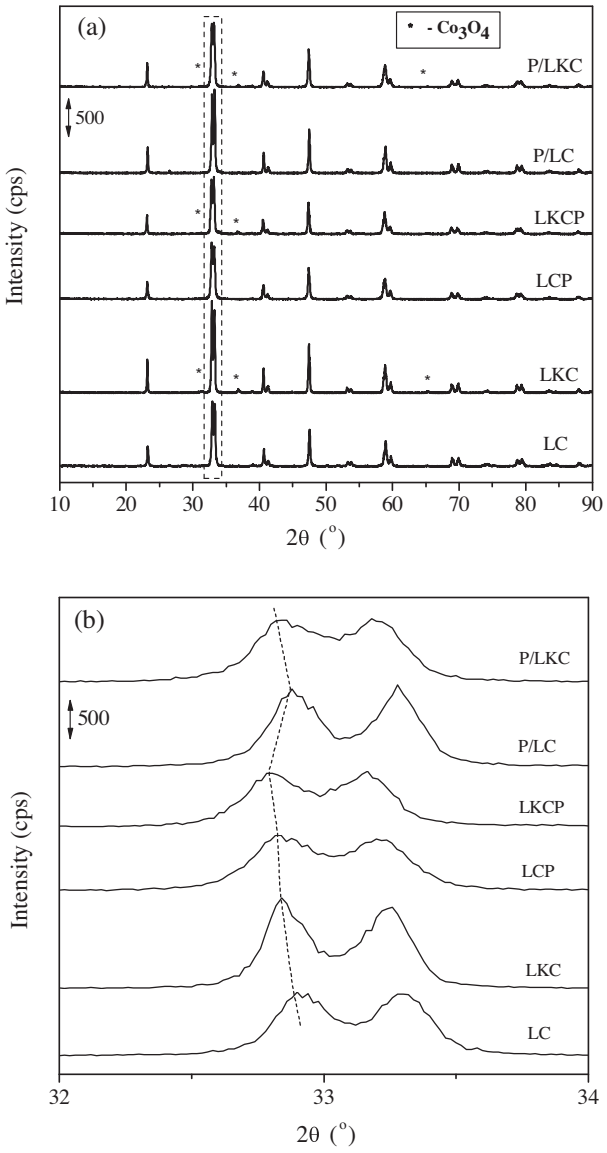

Fig. 1. XRD patterns of $La_{1-x}K_xCo_{1-y}Pd_yO_{3-\delta}$ and $Pd/La_{1-x}K_xCoO_{3-\delta}$ ($x = 0, 0.1$; $y = 0, 0.05$): (a) full patterns and (b) regional enlarged patterns for (1 1 0) and (1 0 4) reflections.

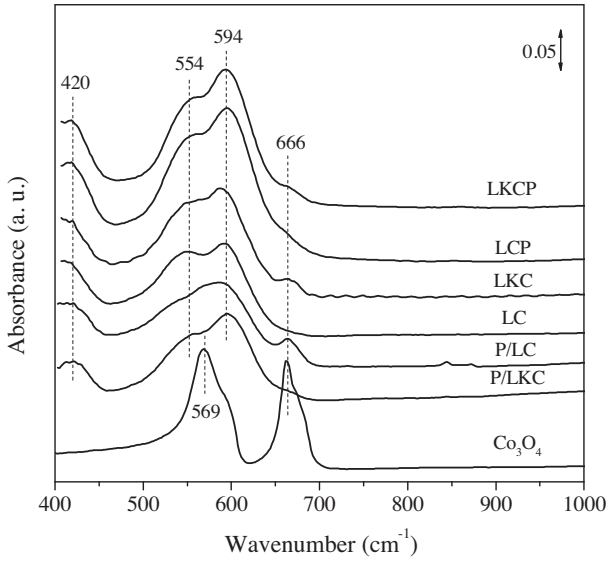

Fig. 2. FT-IR spectra of $La_{1-x}K_xCo_{1-y}Pd_yO_{3-\delta}$ and $Pd/La_{1-x}K_xCoO_3$ ($x = 0, 0.1$; $y = 0, 0.05$).

and LKC, which confirms that Pd ions are hardly introduced into the perovskite lattice by impregnation [18]. For all the samples containing Pd, no diffraction signals related to Pd species are detected, suggesting the high dispersion or small crystallites size of Pd species.

3.1.2. FT-IR

It is well known that the BO_6 octahedron with A-site cation in their clearance is the unit cell of ABO_3 structure. In BO_6 unit, there are six kinds of vibrations in their IR spectra. If three pairs of B—O bonds have the same length, namely, BO_6 octahedron with high symmetry, the stretching vibration is IR inactive. When the symmetry of BO_6 is lowered to some extent, the B—O stretching vibration is IR active [19]. The IR spectra of the as-prepared catalysts are displayed in Fig. 2. Three main characteristic bands appearing at 420, 554 and 594 cm^{-1} are observed in the IR spectra. The band at 420 cm^{-1} corresponds to the bending vibration of Co–O bonding in the BO_6 octahedron, and the bands at 562 and 596 cm^{-1} can be assigned to two kinds of Co–O stretching vibration in the BO_6 octahedron [16,20]. The FT-IR results further prove that the ABO_3 perovskite structures are present and stable after single or dual substitution as well as the impregnation. Compared with K-free samples (LC, LCP, P/LC), it is found that all the K-substituted samples (LKC, LKCP, P/LKC) show a very weak IR band at 666 cm^{-1}, which is attributed to Co_3O_4 phase; in addition, this peak for LKCP is relatively weaker than that for LKC, suggesting that the substitution of Pd can stabilize the Co^{3+} ions in $LaCoO_3$ perovskite structure. These results are totally consistent with those of XRD.

3.1.3. FE-SEM and HRTEM

FE-SEM photographs of the Pd-containing catalysts are presented in Fig. 3. It can be seen that the sphere-like perovskite particles possess the size around 40–70 nm, close to that of diesel soot particulates (30–100 nm), which is favorable to achieving the high specific number of contact points between the two counterparts. Compared with the SEM images for K-free samples (Fig. 3(a), (c) and (e)), those for the K-substituted samples (Fig. 3(b), (d) and (f)) exhibit smaller size or higher dispersion of perovskite crystallites. When Pd is introduced into the catalysts, the similar situation occurs just like K-substitution. Among all the Pd-containing samples, LKCP has the smallest mean crystallite size, which is consistent with that calculated from the XRD results by using Scherrer equation (LCP: 46.5 nm, LKCP: 42.1 nm, P/LC: 66.6 nm, P/LKC: 52.6 nm).

To investigate the existing states of Pd in Pd-containing catalysts LKCP and P/LKC, the technique of high resolution transmission election microscopy (HRTEM) with energy-dispersive X-ray absorption spectroscopy (EDS) was employed to characterize the catalysts morphology, as shown in Fig. 4. In the photograph of LKCP, the lattice fringes spacing of 0.269 nm corresponding to $LaCoO_3$ (1 0 4) plane is clearly observed, but no planes of Pd or PdO phases are found, suggesting that the Pd ions may have incorporated into the lattice of $LaCoO_3$ perovskite structure, which is supported by the XRD results. The homogeneous presence of Pd throughout the entire catalyst LKCP is demonstrated by the very similar EDS results obtained from different nano-particles (EDS results of other nano-particles not shown). To further prove the deduction for the existence of Pd ions in perovskite lattice, the sample LKCP was reduced by H_2 at 200 °C, and then used for HRTEM measurement. Since Pd ions can be readily reduced to Pd^0, and the formed Pd^0 cannot stay in the lattice of perovskite due to electrical neutrality, on perovskite surface there must be detectable Pd^0 phase [21,22]. As shown in Fig. 3(b), the (1 1 1) plane of metallic Pd with a size of ~3 nm is indeed observed after reduction treatment. For the impregnated sample P/LKC, the plane of PdO (1 1 1) is easily detected, suggesting the presence of PdO on perovskite surface, whose size is about 16 nm. The EDS spectrum of P/LKC also indicates that this sample contains much larger amount of Pd element on the surface as compared with the LKCP. In summary, for the dually substituted sample LKCP the Pd ions mainly exist in perovskite lattice, while for the impregnated sample P/LKC the Pd exists in the form of PdO on the perovskite surface.

3.1.4. XPS

The specific oxidation states of Pd species in the catalysts are analyzed by XPS, as shown in Fig. 5. For all samples, there are two main binding energy peaks corresponding to Pd $3d_{3/2}$ and Pd $3d_{5/2}$ levels. The Pd $3d_{5/2}$ binding energy peak for P/LKC catalyst appears at 336.8 eV, attributed to Pd^{2+} [23–25]. The high symmetry of Pd $3d_{5/2}$ peak suggests the relatively homogeneous environment of Pd^{2+} ions. Combined with the HRTEM results, it is deduced that in P/LKC and P/LC samples Pd mainly exists as PdO nanoparticles. Similar assignment was also reported in literatures [26,27]. In contrast, the binding energy peaks of Pd $3d_{3/2}$ and Pd $3d_{5/2}$ for the samples LCP and LKCP appear at higher energy position (0.4 eV higher for Pd $3d_{5/2}$, 0.6–1.5 eV higher for Pd $3d_{3/2}$), indicating that the Pd^{n+} ($n > 2$) ions with higher oxidation states may be present in them [12,21,28–31] which is also confirmed by XANES results in the following section. Considering the relatively low symmetry of the peaks Pd $3d_{5/2}$ and Pd $3d_{3/2}$, the coexistence of different Pd^{n+} ($n > 2$) species in such Pd-substituted samples is potential. Besides, the much larger linewidth of the Pd $3d_{3/2}$ signal for LKCP suggests that there are at least two distinct Pd sites. By careful comparison of the two spectra for LCP and LKCP, it can be found that the binding energy of Pd $3d_{3/2}$ of LKCP catalyst is 0.9 eV higher than that of LCP, implying the higher valence of Pd ions in LKCP. Since the valence of K is much lower than that of La, the substitution of La by K can lead to the formation of Pd with higher oxidation state, and/or the formation of oxygen vacancies so that the electrical neutrality of the perovskite can be maintained. The presence of oxygen vacancies will be further verified by soot-TPR in the following section.

To discuss the oxidation state of Co, the XPS spectra of Co $2p_{3/2}$ core level for Pd-containing catalysts are shown in Fig. 5. The binding energy of Co $2p_{3/2}$ for K-free samples (LC, P/LC, LCP) is about 779.7 eV which is close to the binding energy of Co^{3+} in Co_2O_3 (779.6 eV), while for K singly substituted samples (LKC, P/LKC) the binding energy of Co $2p_{3/2}$ is only 779.3 eV, suggesting the presence of some Co^{4+} ions after La^{3+} ions are partially substituted by K^+ ions. However, for K/Pd dually substituted sample (LKCP), the binding energy of Co $2p_{3/2}$ is 779.5 eV which is between those for K

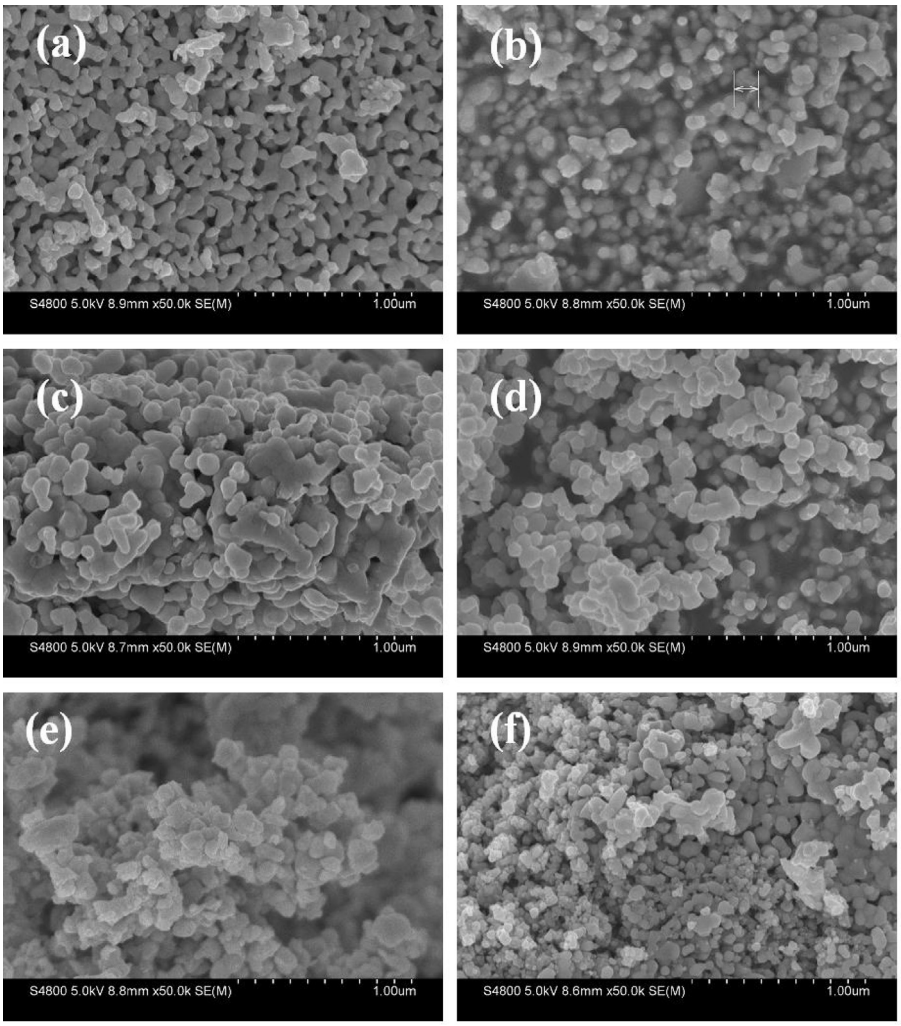

Fig. 3. FE-SEM photographs of the catalysts: (a) LC, (b) LKC, (c) LCP, (d) LKCP, (e) P/LC and (f) P/LKC.

singly substituted samples and K-free samples, which implies that less Co^{4+} ions exist in LKCP due to the simultaneous increase of the oxidation state of substituted Pd ions at B-site. The segregation of Co to form trace Co_3O_4 (detected by XRD and FT-IR) is mainly resulted from K-substitution. Since the valence of K^+ is much lower than that of La^{3+}, the partial substitution of La by K will lead to the increase of the oxidation state of B-site ions (Pd and/or Co) as well as the potential formation of oxygen vacancies so that the electrical neutrality of the perovskite can be maintained.

3.1.5. XANES and EXAFS

To get more information about the coordination environment and the oxidation state of Pd in the catalysts, Pd *K*-edge XANES spectra were recorded. The normalized Pd *K*-edge XANES spectra of the Pd-containing catalysts together with the reference materials PdO and Pd foil are shown in Fig. 6(a). It is seen that the XANES spectra of the prepared samples are quite different from that of Pd foil but close to that of PdO, especially that of P/LKC, which is almost identical to the spectrum of PdO, suggesting the very similar coordination environment of Pd species in these two samples. Small differences between the spectra of the reference PdO and the substituted samples LCP and LKCP are also present: firstly, the *K*-edge absorption curves of Pd ions in LCP and LKCP show a small shift to higher energy position, meaning that the valence of Pd in them is higher than the normal bivalence [11]; secondly, the *K*-edge white lines of Pd ions in LCP and LKCP are a little stronger and obviously split into two peaks, suggesting the not uniform symmetric coordination environment, which is consistent with the above XPS results. It is well known that after substitution of B-site ions the cubic perovskite structure will be distorted to some extent due to the difference in both size and charge between the original B-site ion and the substituting ion. So, it is natural that the Pd ions locating in the distorted cubic perovskite show relatively lower symmetry than those for the impregnated sample P/LKC. To display the edge shift more clearly, the first and second derivative of the XANES spectra were calculated and shown in Fig. 6(b) and (c), respectively. It is reported that [29,32] the second derivative curve can be used to identify the fine features in the edge region and to locate them more accurately on energy. In Fig. 6(c) three peaks around the white lines are identified, whose positions are strongly dependent on the valence of Pd, and the details of assignment could be found in literature [32]. From Fig. 6(c), it is found that the peak A only appears in the curves of PdO and P/LKC, which implies that the Pd ions in P/LKC are bivalent and possess square-planar symmetry because this shoulder peak is regarded as the characteristic peak of Pd^{2+} with square-planar symmetry. However, nearly no peak A is found for LCP and LKCP, suggesting the absence of bivalent Pd ions. The position of peak B for P/LKC is almost same as that for PdO, while that for LCP and LKCP is about 2 eV higher. It is reported [29] that peak B for Pd^{4+} with octahedral coordination (e.g. Zn_2PdO_4) often appears at higher position, which is about 3 eV higher than that for Pd^{2+} with square-planar coordination (e.g. PdO) and Pd^{3+}

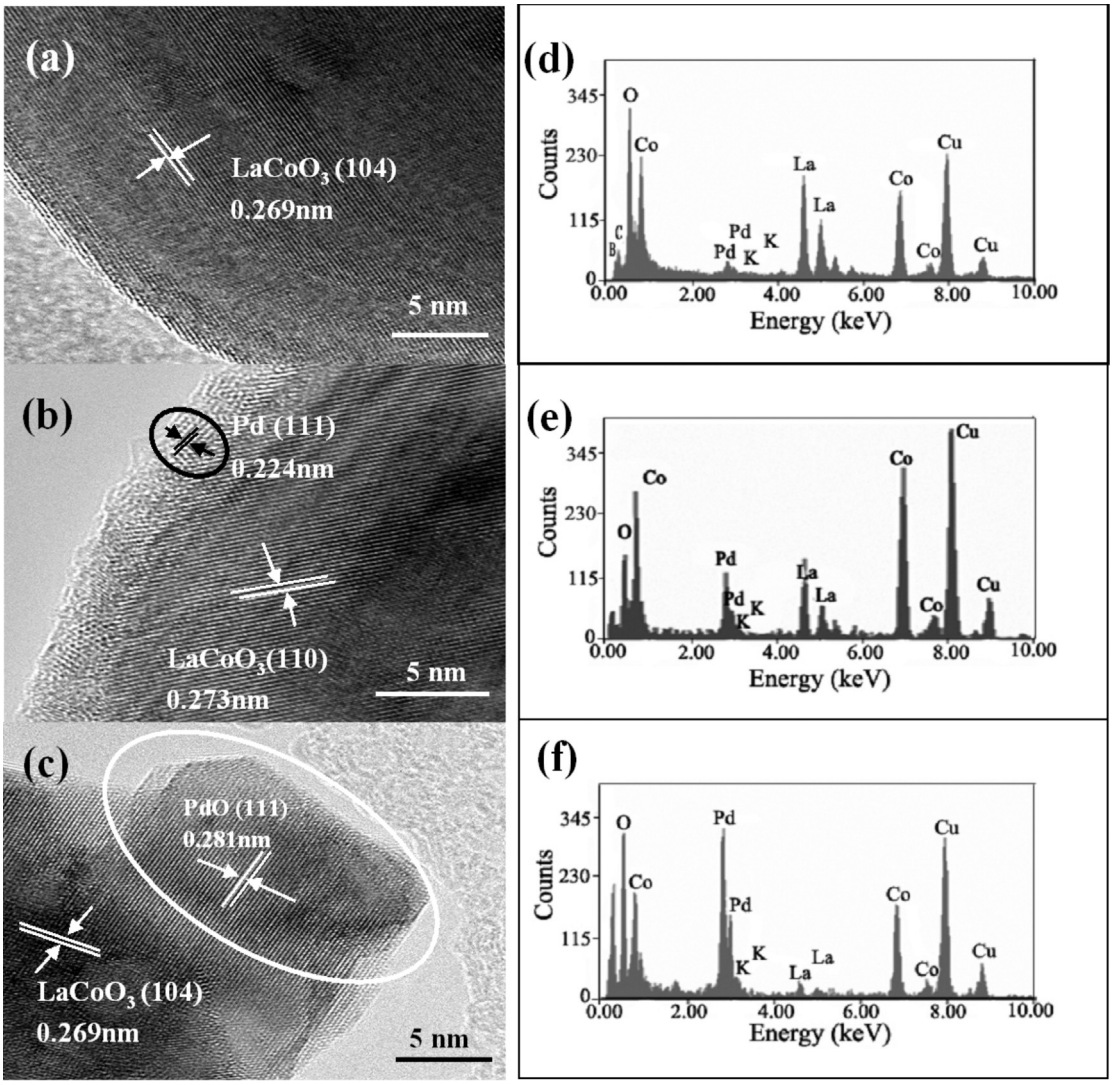

Fig. 4. HRTEM photographs and EDS spectra of the catalysts: (a) and (d) for LKCP; (b) and (e) for LKCP pre-reduced by H_2 at 200 °C; (c) and (f) for P/LKC.

with distorted octahedral coordination (e.g. $LaPdO_3$). In this work, only ~2 eV shift of peak B is observed for LCP and LKCP, implying that some but not all of the Pd ions in them are tetravalent. The last peak C appearing at the position about 12 eV higher than peak B, is also sensitive to Pd valence [29]; higher valence corresponds to larger intensity. In Fig. 6(c), LCP and LKCP obviously show much stronger peaks C than pure PdO and P/LKC; in addition, LKCP exhibits a little higher intensity of peak C than LCP, meaning that more tetravalent Pd ions exist in LKCP. The co-existence of monovalent K ions may cause the increase of the valence of Pd ions. This deduction is consistent with the XPS results. In a word, Pd species in P/LKC mainly existing as PdO nanoparticles are bivalent ions which possess square-planar symmetry; while those in LCP and LKCP show higher valence such as trivalence and/or tetravalence, which possess distorted octahedral coordination symmetry.

The radial distribution functions (RDFs) of Pd *K*-edge obtained by Fourier transform of the EXAFS data are shown in Fig. 7, in order to further demonstrate the formation of solid solution between Pd and perovskites for the samples LCP and LKCP. The RDF of Pd foil shows only one coordination peak at 2.49 Å referred to Pd–Pd coordination shell. The RDF of PdO exhibits two major coordination peaks appearing at 1.56 Å and 2.85 Å, attributed to Pd–O shell and Pd–Pd shell, respectively. The impregnated sample P/LKC shows similar RDF to PdO except that the long-range R-space peaks for PdO and P/LKC are not in the same position. This does not preclude the existence of nanoparticulate PdO since the appearance of the long-range peaks strongly depends on the particle size due to interference between the paths. The sample P/LKC shows a little larger distance for Pd–Pd shell, suggesting that the Pd in this sample is highly dispersed as compared with those in bulk PdO. However, the RDFs for the substituted samples LCP and LKCP display only one coordination peak at about 1.56 Å. The absence of the second coordination peaks (Pd–Pd shell) indirectly demonstrates that no PdO crystallites exist in the substituted samples; on the contrary, the Pd ion may be individually incorporated into the lattice of $LaCoO_3$ perovskite, forming uniform solid solution between Pd and perovskites [33–35].

3.1.6. H_2-TPR

The reducibility of the catalysts was characterized by H_2-TPR, as displayed in Fig. 8. The catalysts LC and LKC show similar reduction profiles containing two main peaks, which correspond to the stepwise reduction of $LaCoO_3$ perovskites; the lower reduction peak (300–450 °C) is attributed to the reduction of Co^{3+} to Co^{2+}, forming oxygen-deficient perovskite (La_2CoO_4), and the higher reduction peak (480–620 °C) is assigned to the further reduction of La_2CoO_4 to Co^0 and La_2O_3 [10]. After partially substituted by Pd, a weak shoulder peak (below 130 °C) emerges for the catalysts LCP and

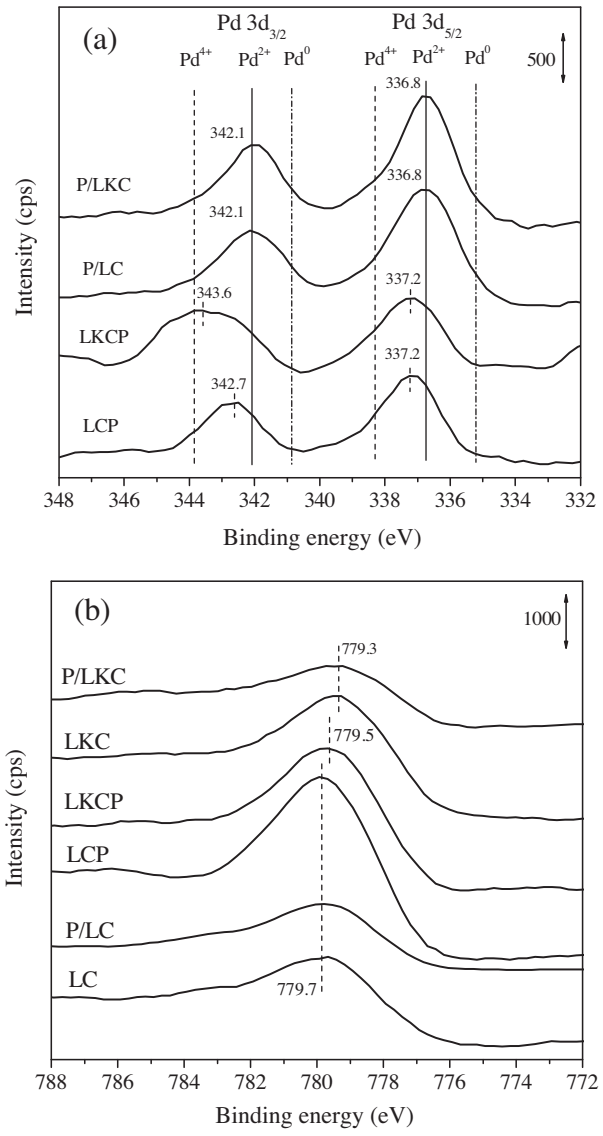

Fig. 5. XPS spectra of (a) Pd 3d core levels of the catalysts LCP, LKCP and P/LKC, and (b) Co $2p_{3/2}$ core levels of all the catalysts.

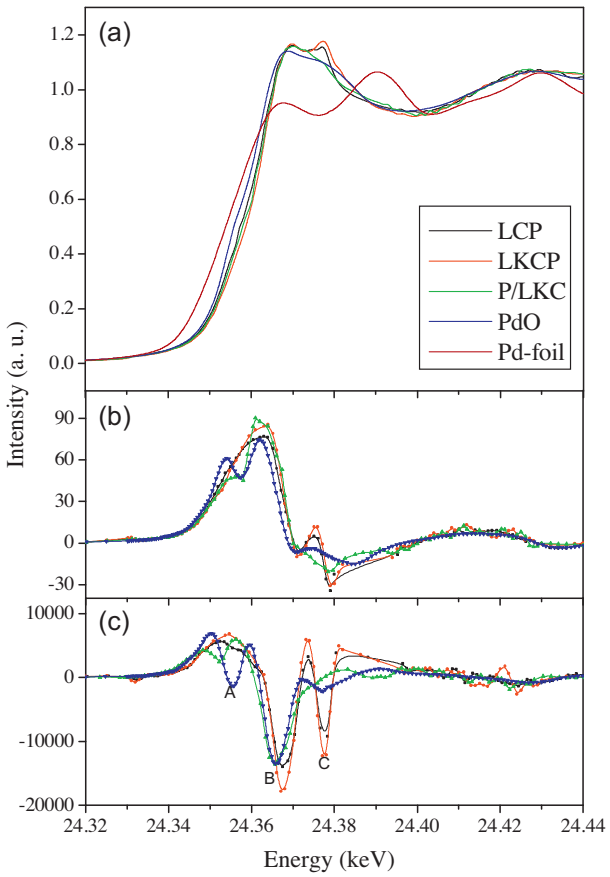

Fig. 6. (a) Normalized Pd *K*-edge XANES spectra of the catalysts $La_{1-x}K_xCo_{0.95}Pd_{0.05}O_{3-\delta}$ and $Pd/La_{0.9}K_{0.1}CoO_3$ ($x = 0$, 0.1) as well as the references PdO and Pd foil; (b) the first derivative curves of the spectra in (a); (c) the second derivative curves of the spectra in (a).

LKCP, owing to the reduction of Pd ions [36,37]; the co-existence of K increases the reduction of Pd ions in perovskite structure, further decreasing the reduction temperature and increasing the reduction area of the shoulder peak. According to XANES results, the presence of low-valence K ions in perovskite can increase the amount of tetravalent Pd ions, which naturally consume more H_2 during TPR. In addition, more evidences are provided to verify this peak related to the reduction of Pd as shown in Fig. S2, Table S2 and Discussion S1. The next two main peaks are also assigned to the successive two-step reduction of $LaCoO_3$ perovskites [38,39]. It should be noted that the substitution of Pd can enhance the reduction processes, making the first main reduction peak remarkably shift to the lower temperature. Hydrogen spillover arising from the as-formed metallic Pd can well account for this enhancement effect [40]. For the impregnated samples P/LC and P/LKC, the first shoulder peak appears at a little higher temperature as compared with that of substituted samples, suggesting that the Pd^{n+} ($n > 2$) ions with octahedral coordination symmetry in Pd-substituted catalysts are easier to be reduced than the Pd^{2+} ions with square-planar coordination symmetry in impregnated samples. In summary, the reducibility of Pd species in these perovskite catalysts changes in the following sequence: LKCP > LCP > P/LKC > P/LC > LKC > LC.

3.1.7. Soot-TPR

For catalytic oxidation reaction, the study of the surface oxygen species is highly necessary, so, soot-TPR was carried out in highly pure N_2 (99.99%) atmosphere. In this condition, soot can only be

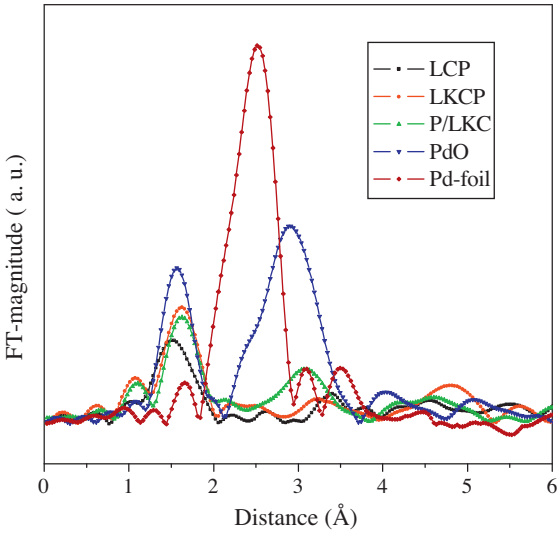

Fig. 7. Pd *K*-edge radial distribution functions of the catalysts derived from EXAFS.

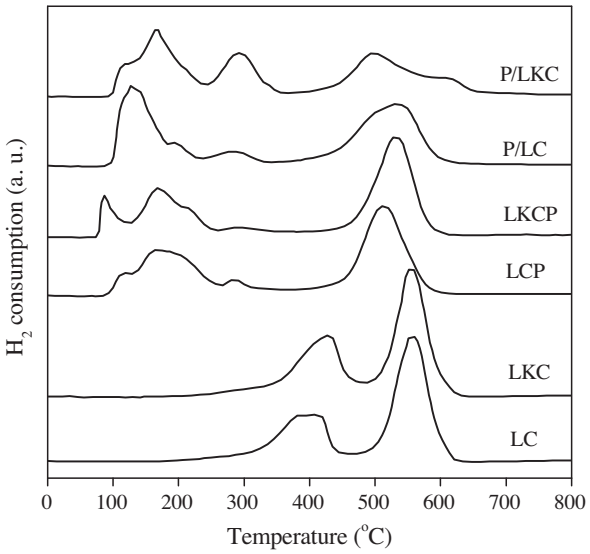

Fig. 8. H_2-TPR profiles of the prepared catalysts.

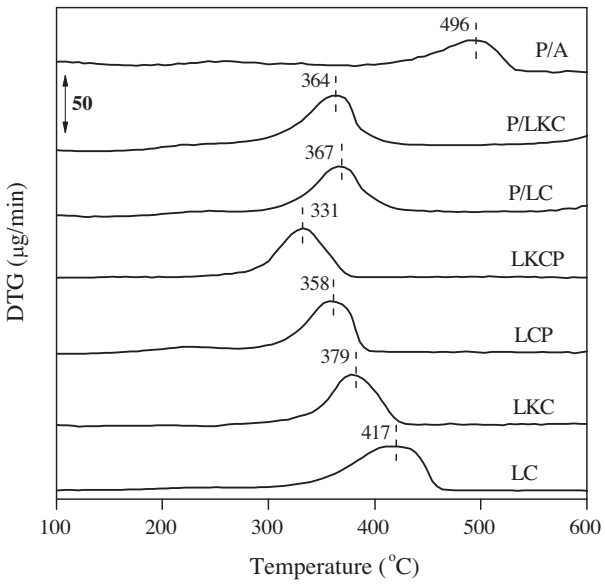

Fig. 10. DTG profiles of soot combustion over the prepared catalysts in the atmosphere of 600 ppm NO + 10 vol.% O_2 + N_2.

oxidized by the surface oxygen species of the catalysts including surface adsorbed oxygen and surface lattice oxygen. Fig. 9 shows the soot-TPR profiles, which are divided into three temperature regions, corresponding to the three kinds of oxygen species namely O_2^- (320–440 °C), O^- (440–670 °C) and O^{2-} (>625 °C) according to literature [41,42]. The reduction temperature for lattice oxygen is much higher than other oxygen species, indicating its poor reactivity with soot. Considering the low soot ignition temperature (<400 °C) in this work (see the next section), it is inferred that the surface chemisorbed oxygen species (O_2^-, O^-) should be the main active oxygen species for soot combustion. Generally, the surface adsorbed oxygen species (O_2^-, O^-) are produced through the adsorption of gaseous O_2 on the oxygen vacancies. In view of the approximate areas for second reduction regions, it is clear that the LKCP sample possesses the largest amount of surface adsorbed oxygen species, reflecting its largest amount of oxygen vacancies resulted from the dual-substitution of K and Pd. The soot-TPR results can be well correlated with the soot combustion activity described in the next section.

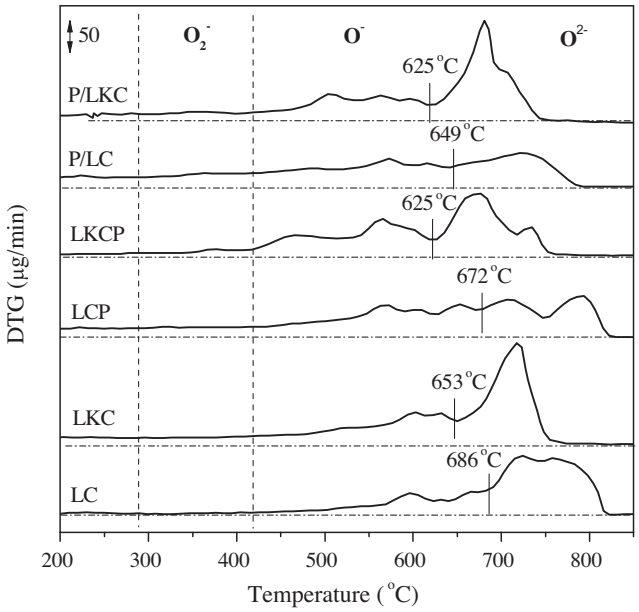

Fig. 9. DTG profiles of soot-TPR over the prepared catalysts.

3.2. Catalytic soot combustion

The catalytic performance of $La_{1-x}K_xCo_{1-y}Pd_yO_{3-\delta}$ and $Pd/La_{1-x}K_xCoO_{3-\delta}$ for soot combustion in the atmosphere of 600 ppm NO, 10 vol.% O_2 and N_2 is shown in Fig. 10 and Table 1. As seen from Table 1, the uncatalyzed soot combustion starts from 438 °C with a T_m as high as 610 °C, while over LC catalyst soot combustion starts from 303 °C with the T_m lowered to 417 °C. When $LaCoO_3$ is partially substituted by K or Pd separately, the T_m is further decreased by 38 °C and 59 °C, respectively. The enhanced activity of K-substituted sample could be ascribed to the improved contact condition between catalyst and soot, and the formation of more oxygen vacancies due to the much lower valence of K^+ than La^{3+}, while the promotional effect of the substitution by Pd on the activity is attributed to not only the generation of oxygen vacancies but also the arising of additional active sites of Pd itself. If K and Pd are simultaneously introduced to the structure of $LaCoO_3$ perovskite, the T_m is greatly decreased to 331 °C, implying a synergetic effect of K and Pd in the catalyst. Firstly, the simultaneous substitution increases the specific surface area, the number of oxygen vacancy and the amount of surface adsorbed oxygen species of the catalyst; secondly, the simultaneous substitution is favorable to the formation of high-valence Pd ions (trivalent and/or tetravalent) as revealed by XPS, XANES and EXAFS, improving the reducibility of the catalyst; thirdly, the simultaneous substitution can enhance the formation of perovskite structure, inhibiting the formation of Co_3O_4 (see XRD and FT-IR); fourthly, the substituted Pd ions exist as solid solution, greatly increasing the dispersion of Pd species, as a result, the oxidation sites may be also increased. For comparison, the traditional supported catalyst Pd/Al_2O_3 (denoted as P/A) with the same Pd loading of 2.1 wt.% was also prepared by the same method as $Pd/La_{1-x}K_xCoO_{3-\delta}$, and used for soot combustion. It is found that this catalyst shows much lower activity (T_m = 496 °C) than the Pd-substituted perovskite catalyst. Apparently, the existence of Pd in K-promoted $LaCoO_3$ perovskite can more efficiently exert the function of Pd. According to the T_m, the catalytic soot oxidation activities of different catalysts could be arranged in the following

Table 1
Specific surface area (SSA), characteristic temperatures, the activation energy (E_a) and the NOx reduction efficiency (NRE) during soot combustion over $La_{1-x}K_xCo_{1-y}Pd_yO_{3-\delta}$ and $Pd/La_{1-x}K_xCoO_3$ catalysts.

Catalysts	SSA (m^2/g)	T_i (°C)	T_m (°C)	T_f (°C)	E_a (kJ/mol)	NRE (%)
LC	6.5	303	417	466	101.5	10.0
LKC	6.9	291	379	430	99.0	18.5
LCP	10.2	267	358	401	99.6	17.8
LKCP	11.1	219	331	387	93.6	26.7
P/LC	9.7	287	367	436	124.4	15.5
P/LKC	10.5	262	364	425	115.9	19.7
P/A	149.6	226	496	538	113.1	–
Uncatalyzed	–	438	610	660	145.0	–

order: LKCP > LCP > P/LKC > P/LC > LKC > LC > P/A. On the whole, the Pd-containing samples show much higher catalytic activity for soot combustion as compared with Pd-free ones. Among these Pd-containing samples, the Pd-substituted perovskites are more active than the Pd-impregnated ones, further demonstrating that the coordination environment and the chemical states of Pd ions are crucial to the catalytic activity. The detailed reaction mechanism for soot combustion over Pd-containing catalysts will be discussed subsequently.

To further confirm the role of Pd in the substituted perovskites, two series of catalysts with different amounts of palladium ($LaCo_{1-y}Pd_yO_{3-\delta}$ and $La_{0.9}K_{0.1}Co_{1-y}Pd_yO_{3-\delta}$, $y = 0, 0.01, 0.03, 0.05$) were prepared (denoted as LCP-y or LKCP-y) and employed for soot combustion just for a comparison, the results of which are shown in Fig. 11. For both series of catalysts, the catalytic activity is increasing with the increase of substitution amounts of palladium. When the amount of palladium reaches $y = 0.05$ (~2.1 wt%), the lowest T_m of 358 and 331 °C for $LaCo_{0.95}Pd_{0.05}O_{3-\delta}$ and $La_{0.9}K_{0.1}Co_{0.95}Pd_{0.05}O_{3-\delta}$ in each series of catalysts is achieved, which is about 25 and 21 °C lower than that for the samples with $y = 0.01$, respectively. Therefore, it is concluded that the amount of substituted Pd in perovskites directly influences the catalytic activity.

The effects of NOx and O_2 on soot combustion were also investigated on the LKCP catalyst by changing the reaction atmospheres, the results of which are shown in Fig. 12. In pure N_2 (99.99%), soot can only be oxidized by the surface adsorbed oxygen species (O_2^-, O^-) and surface lattice oxygen (O^{2-}) of the catalysts. The very tiny peak at 371 °C may correspond to the soot oxidation by surface adsorbed oxygen (O_2^-, O^-), while the others at much higher temperature may arise from the soot oxidation by surface lattice oxygen (O^{2-}) which is much more stable than adsorbed oxygen species. When O_2 is introduced, the tiny peak is greatly increased with the temperature unchanged but the maximal soot combustion rate increased remarkably, as displayed in Fig. 12b. This result implies that O_2 in the atmosphere could be continuously activated on the same oxygen vacancies and converted into surface active oxygen species (O_2^-, O^-) so that the soot combustion could take place continuously. When NO is introduced into pure N_2 without O_2, although the peak temperature for soot combustion is decreased a little, the peak intensity is lower and the range between T_i and T_f is wider as compared with those in pure N_2 atmosphere shown in Fig. 12c. It suggests that in the absence of oxygen the small amount of NO does not show strong reactivity with soot. In the presence of both NO and O_2, much better activity for soot combustion is achieved, showing not only low T_m but also large combustion rate as seen in Fig. 12d. Since NO can be oxidized to NO_2 by both surface oxygen species (O_2^-, O^-) and gaseous O_2 [4,43], it is deduced that the high catalytic activity may be mainly contributed by the reaction between NO_2 and soot. To prove this deduction, the soot combustion is also studied in the $NO_2 + N_2$ atmosphere, as shown in Fig. 12e. It is found that little difference exists between the two curves (Fig. 12d and e), suggesting the correctness of the above supposition. In addition, the catalytic activity in the atmospheres of $NO_2 + O_2$ and $NO + O_2$ balanced by N_2 (Fig. 12d and f) are almost the same, further demonstrating that the soot combustion mechanism via the route of NO_2 in $NO + O_2$ atmosphere is reliable.

The NOx reduction efficiency (NRE) is also calculated by comparing the differences between the amounts of adsorbed and desorbed NOx over the catalysts mixed with soot, which has been reported elsewhere [44]. The calculated results of NRE in the reaction temperature region of 100–700 °C are listed in Table 1. As seen from this table, the NRE decreases in the following order: LKCP > P/LKC > LKC > LCP > P/LC > LC. The NREs of K-substituted

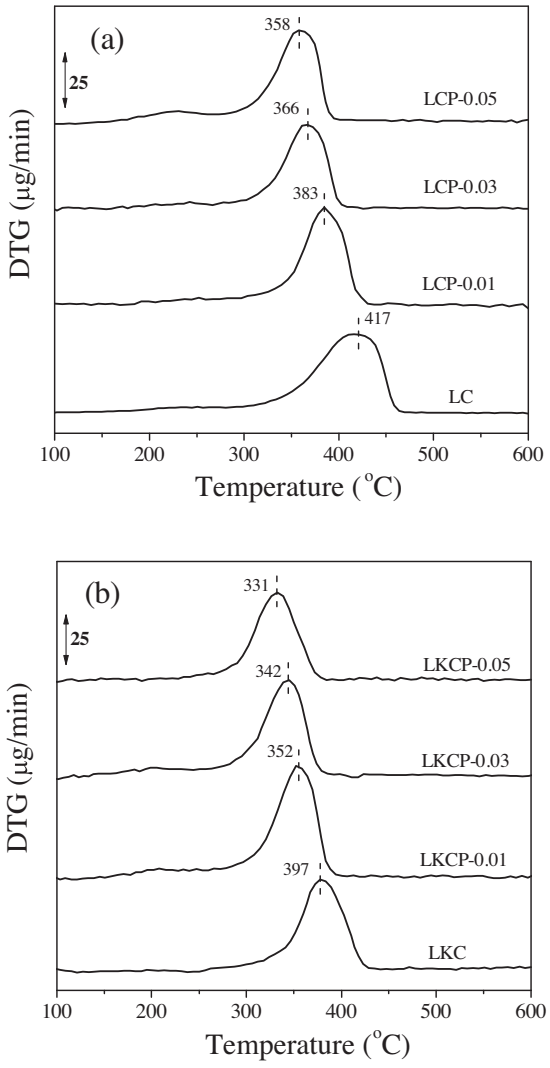

Fig. 11. DTG profiles of soot combustion over the catalysts: (a) $LaCo_{1-y}Pd_yO_{3-\delta}$ ($y = 0, 0.01, 0.03, 0.05$) and (b) $La_{0.9}K_{0.1}Co_{1-y}Pd_yO_{3-\delta}$ ($y = 0, 0.01, 0.03, 0.05$) in the atmosphere of 600 ppm NO + 10 vol.% $O_2 + N_2$.

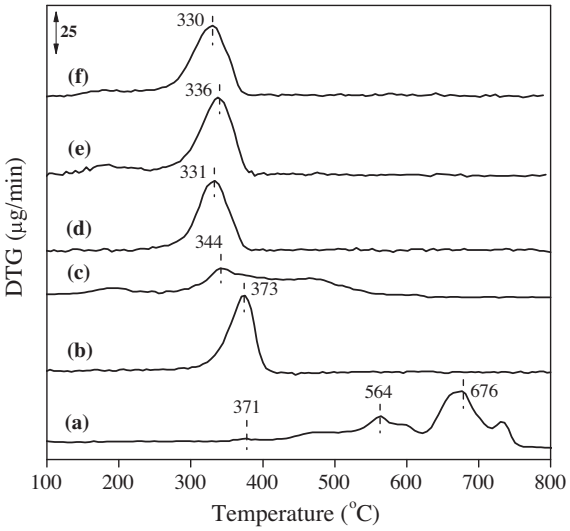

Fig. 12. DTG profiles of soot combustion over the catalyst $La_{0.9}K_{0.1}Co_{0.95}Pd_{0.05}O_3$ in different atmospheres: (a) pure N_2, (b) 10 vol.% $O_2 + N_2$, (c) 600 ppm NO + N_2, (d) 600 ppm NO + 10 vol.% $O_2 + N_2$, (e) 400 ppm $NO_2 + N_2$ and (f) 400 ppm NO_2 + 10 vol.% $O_2 + N_2$.

perovskites are larger than K-free samples since the strong basicity of K is favorable to trapping the acidic NOx. The Pd-containing perovskites possess higher NREs than Pd-free samples, probably due to the higher capability of Pd for the adsorption of NO and its oxidation to NO_2. Meanwhile, the Pd-substituted perovskites also show higher NREs than the supported Pd catalysts (LKCP > Pd/LKC; LCP > P/LC), which suggests that Pd^{n+} ($n > 2$) ions in perovskites possess higher oxidibility for NO oxidation to NO_2 and the subsequent NOx reduction by soot as compared with Pd^{2+} in supported catalysts.

In order to seek the experimental proofs of NO_2 involved in soot combustion over the catalyst LKCP, the NO_2 concentration was monitored during the temperature programmed reaction in 600 ppm NO + 10 vol.% $O_2 + N_2$ in the absence or presence of soot, as shown in Fig. 13 (black lines: only catalyst exist; red lines: catalyst and soot co-exist). The difference between the NO_2 concentrations in the presence of catalysts and that in the presence of catalysts plus soot at any temperature is defined as the reactive NO_2 (blue line), which has reacted with soot during the reaction. From Fig. 13(a), it is observed that over LKCP catalyst the temperature range for the reactive NO_2 is in good agreement with that for soot combustion shown in the DTG profile (light magenta line). When the reactive NO_2 reaches the maximum, the concentration of NO is close to zero (not shown in this figure). So, it is inferred that NO_2 is produced from NO oxidation, which acts as the main oxidizer for soot combustion. For comparison, the NO_2 concentration for the Pd-free catalyst LKC was also monitored by the similar method. It is found that for LKC samples the NO_2 concentration in the absence of soot is really lower than that for LKCP, suggesting the higher capability of LKCP for NO oxidation to NO_2. In the presence of LKC + soot, the reactive NO_2 concentration is also much lower than that for LKCP + soot. All these results indicate that the existence of Pd in perovskite structure enhances not only the oxidation of NO but also the combustion of soot, which directly evidences the involvement of NO_2 and Pd in soot combustion reaction.

Combined with all the results of catalyst characterization and analysis of reaction path, a potential mechanism scheme for soot combustion over LKCP catalyst in the NO-containing atmosphere (600 ppm NO + 10 vol.% $O_2 + N_2$) is proposed, as displayed in Fig. 14. There are two reaction pathways for soot oxidation namely the

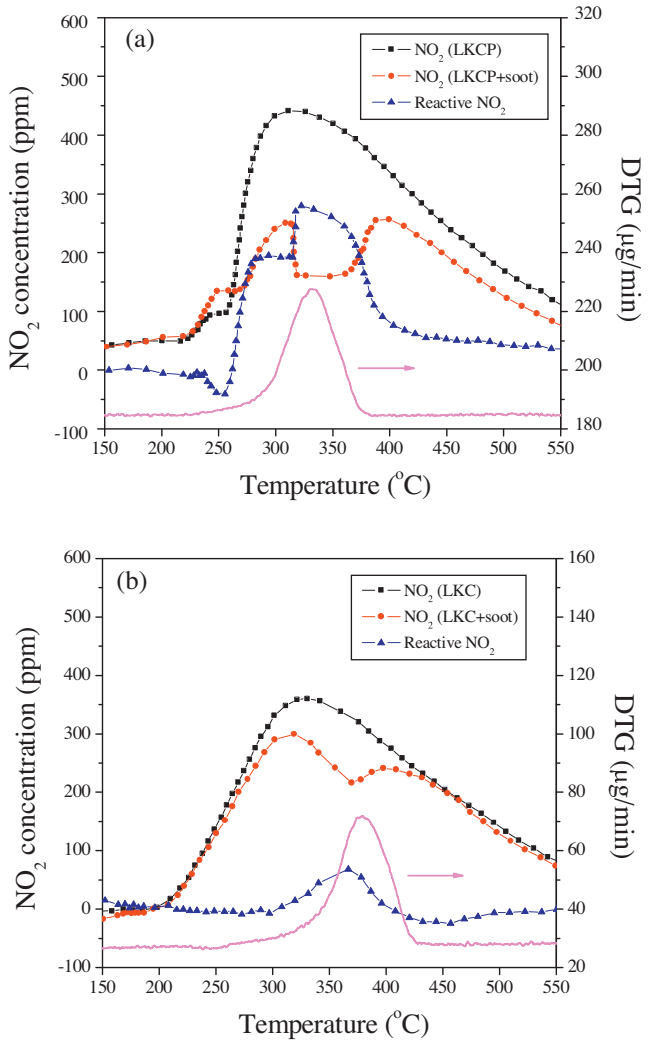

Fig. 13. Concentration curves of NO_2 and the DTG profile for (a) LKCP and (b) LKC catalyst or the catalyst mixed with soot in the atmosphere of 600 ppm NO + 10 vol.% $O_2 + N_2$.

direct oxidation by oxygen via the oxygen vacancies and the NO_2-assisted soot oxidation. For direct oxidation route, soot is oxidized on the solid–solid interface between the catalyst and soot by the adsorbed active oxygen species (O^{2-} and O^-), which can be continuously supplemented by gaseous O_2 through the oxygen vacancies, while for NO_2-assisted oxidation of soot, NO is firstly captured by the perovskite catalyst and subsequently oxidized into NO_2 by the surface active oxygen species [4–6], during this stage the Pd sites with high oxidation capability play the main role for NO oxidation; then the formed NO_2 reacts with soot to produce N_2 and

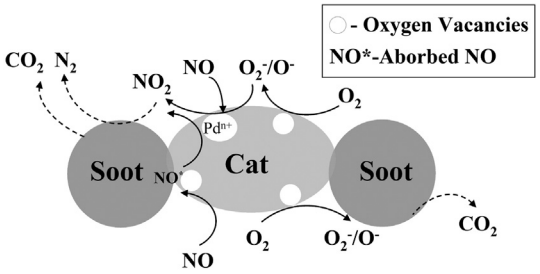

Fig. 14. Scheme of potential reaction pathways for soot combustion in NOx-containing atmosphere over $La_{0.9}K_{0.1}Co_{0.95}PdO_{3-\delta}$ catalyst.

CO_2. For the later reaction path, NO could be captured by both the Pd sites and the oxygen vacancies, forming active adsorbed NOx species. Due to the high oxidibility of Pd^{n+} ($n > 2$) in Pd-substituted perovskites, NO_2-assisted soot combustion should be the dominant reaction path over these samples. In comparison, on supported Pd catalysts (Pd/LC, Pd/LKC and Pd/Al_2O_3), less NO_2 could be formed owing to the weaker capability of Pd^{2+} for NO oxidation, decreasing the enhancement effect of NOx to soot combustion. So, it is obvious that incorporating Pd into perovskite structure is an effective way to exert the advantages of both noble metals and perovskites during soot combustion. In the whole process of soot combustion, the selectivity of soot to CO_2 is as high as 99.5%. It is well known that on different catalysts the activation and reaction pathway may be different, which largely determines the difference in catalytic performance between catalysts. In order to better understand the superior performance of the dually substituted perovskite catalysts $La_{1-x}K_xCo_{1-y}Pd_yO_{3-\delta}$, we performed a series of kinetic experiments and calculated the activation energy of different catalysts for soot oxidation, as listed in Table 1. It is obvious that the activation energy for catalytic soot combustion is much lower than that without using catalysts. The K-substituted samples (LKC, LKCP, P/LKC) always displays lower activation energy than K-free ones (LC, LCP, P/LC). After simultaneous substitution of La and Co by K and Pd, the activation energy of soot combustion is further lowered to a significant extent; the catalyst $La_{0.9}K_{0.1}Co_{0.95}Pd_{0.05}O_3$ exhibits the lowest activation energy (93.6 kJ/mol), which could be well correlated with its highest performance for soot combustion. However, it should be noted that the Pd-impregnated samples P/LKC and P/LC show relatively high activation energy than the perovskite supports LKC and LC, respectively, suggesting that the supported PdO nanoparticles with relatively large size can hardly exert the intrinsic advantage of Pd for NO oxidation and soot combustion. On the contrary, the loading of PdO may cover some of the active sites of perovskites and decrease the contact efficiency between soot and the perovskites; as a result, the activation energy of the supported Pd catalysts is increased to a little extent. On the basis of previous characterizations, it is easily drawn that the Pd ions with high valence (Pd^{3+}, Pd^{4+}) in the perovskite structure are much more favorable to NO oxidation and soot combustion as compared with the supported bivalent PdO species.

The K/Pd dually substituted perovskite catalyst LKCP also possesses high structural stability during soot combustion. After it was used in soot combustion for 5 times, this catalyst still shows almost the same structures as the fresh one, as revealed by XRD and XANES in the Supplementary Data (Fig. S3 and Fig. S4). The thermal stability of $La_{0.9}K_{0.1}Co_{0.95}Pd_{0.05}O_{3-\delta}$ was also investigated by calcination of this sample at 800 °C for 20 h, and compared with that of Pd/Al_2O_3 calcined at the same condition. The TEM images in Fig. S5(a) show that after calcination the LKCP still shows uniform size of about 50 nm, close to the fresh one (~42 nm), meanwhile, no obvious particles of Pd are observed in the HRTEM image of this sample as shown in Fig. S5(b), which suggests that no obvious sintering has taken place on this sample; on the contrary, for the conventional supported catalyst Pd/Al_2O_3, from its TEM images shown in Fig. S5(c) and (d), it is clearly observed that most PdO particles have sintered seriously after calcination and the size of PdO particles has increased up to about 85 nm. In a word, the Pd-substituted perovskite catalyst possesses much higher thermal stability than the supported Pd/Al_2O_3.

4. Conclusion

Simultaneous substitution of La and Co by K and Pd in $LaCoO_3$ perovskite is successfully achieved, the as formed $La_{0.9}K_{0.1}Co_{0.95}Pd_{0.05}O_{3-\delta}$ catalyst exhibits particularly high catalytic performance, showing the lowest characteristic temperatures and lowest activation energy for soot combustion in the presence of NOx. The dually substituted sample possesses the largest specific surface area, the best reducibility and the highest oxidibility to NO oxidation. The simultaneous substitution of K and Pd can generate more active surface oxygen species. The Pd ions with high valence (Pd^{3+}, Pd^{4+}) in distorted octahedral coordination environment are much more active for NO oxidation and soot combustion than the bivalent Pd ions with square-planar coordination symmetry. Two reaction pathways for soot oxidation namely the direct oxidation by the activated oxygen species via oxygen vacancies and the NO_2-assisted soot oxidation are identified. The presence of high-valence Pd ions in perovskite structure greatly increases the concentration of reactive NO_2 species during the reaction, enhancing soot combustion via the second reaction route. The as-prepared dually substituted perovskite catalyst $La_{0.9}K_{0.1}Co_{0.95}Pd_{0.05}O_{3-\delta}$ is promising for the application in real diesel exhaust purification.

Acknowledgements

This work is financially supported by the National Natural Science Foundation of China (No. 21076146, 21276184, 21077043), the Specialized Research Fund for the Doctoral Program of Higher Education of China (No. 20120032110014) and the Program of New Century Excellent Talents in University of China (No. NCET-07-0599). The authors are also grateful to the support from the Program for Introducing Talents of Discipline to Universities of China (No. B06006).

Appendix A. Supplementary data

Supplementary data associated with this article can be found, in the online version, at http://dx.doi.org/10.1016/j.apcatb.2013.05.036.

References

[1] R.H. Hammerle, D.A. Ketcher, R.W. Horrocks, G. Lepperhoff, G. Hüthwohl, B. Lüers, SAE Paper (1994) 942043.
[2] B.A.A.L. van Setten, M. Makkee, J.A. Moulijn, Catalysis Reviews 43 (2001) 489–564.
[3] M.M. Maricq, Journal of Aerosol Science 38 (2007) 1079–1118.
[4] J. Oi-Uchisawa, A. Obuchi, R. Enomoto, J. Xu, T. Nanba, S. Liu, S. Kushiyama, Applied Catalysis B 32 (2001) 257–268.
[5] J. Oi-Uchisawa, A. Obuchi, S.D. Wang, T. Nanba, A. Ohi, Applied Catalysis B 43 (2003) 117–129.
[6] A. Setiabudi, M. Makkee, J.A. Moulijn, Applied Catalysis B 42 (2003) 35–45.
[7] S.S. Hong, G.D. Lee, Catalysis Today 63 (2000) 397–404.
[8] Z.Q. Li, M. Meng, Q. Li, Y.N. Xie, T.D. Hu, J. Zhang, Chemical Engineering Journal 164 (2010) 98–105.
[9] Z.Q. Li, M. Meng, F.F. Dai, T.D. Hu, Y.N. Xie, J. Zhang, Fuel 93 (2012) 606–610.
[10] Z.Q. Li, M. Meng, Y.Q. Zha, F.F. Dai, T.D. Hu, Y.N. Xie, J. Zhang, Applied Catalysis B 121–122 (2012) 65–74.
[11] Y. Nishihata, J. Mizuki, T. Akao, H. Tanaka, M. Uenishi, M. Kimura, T. Okamoto, N. Hamada, Nature 418 (2002) 164–166.
[12] H. Tanaka, I. Tan, M. Uenishi, M. Taniguchi, M. Kimura, Y. Nishihata, J.I. Mizuki, Journal of Alloys and Compounds 408–412 (2006) 1071–1077.
[13] H. Tanaka, M. Taniguchi, M. Uenishi, N. Kajita, I. Tan, Y. Nishihata, J. Mizuki, K. Narita, M. Kimura, K. Kaneko, Angewandte Chemie International Edition in English 45 (2006) 5998–6002.
[14] H. Tanaka, M. Uenishi, M. Taniguchi, I. Tan, K. Narita, M. Kimura, K. Kaneko, Y. Nishihata, J. Mizuki, Catalysis Today 117 (2006) 321–328.
[15] L. Marchetti, L. Forni, Applied Catalysis B 15 (1998) 179–187.
[16] N. Merino, B. Barbero, P. Grange, L. Cadus, Journal of Catalysis 231 (2005) 232–244.
[17] T. Ozawa, Journal of Thermal Analysis 2 (1970) 301–324.
[18] R.D. Shannon, Acta Crystallographica A32 (1976) 751–767.
[19] K.B. Li, X.J. Li, K.G. Zhu, J.S. Zhu, Y.H. Zhang, Journal of Applied Physics 81 (1997) 6943–6947.
[20] D.F. Boltz, M.G. Mellon, Analytical Chemistry 48 (1976) 196–216.
[21] X. Zhang, H. Li, Y. Li, W. Shen, Catalysis Letters 142 (2011) 118–123.

[22] M.B. Katz, G.W. Graham, Y. Duan, H. Liu, C. Adamo, D.G. Schlom, X. Pan, Journal of the American Chemical Society 133 (2011) 18090–18093.
[23] D.H. Kim, S.I. Woo, O.B. Yang, Applied Catalysis B 26 (2000) 285–289.
[24] D.L. Mowery, M.S. Graboski, T.R. Ohno, R.L. McCormick, Applied Catalysis B 21 (1999) 157–169.
[25] K.R. Priolkar, P. Bera, P.R. Sarode, M.S. Hegde, S. Emura, R. Kumashiro, N.P. Lalla, Chemistry of Materials 14 (2002) 2120–2128.
[26] K. Zhou, H. Chen, Q. Tian, Z. Hao, D. Shen, X. Xu, Journal of Molecular Catalysis A: Chemical 189 (2002) 225–232.
[27] J.P. Dacquin, C. Dujardin, P. Granger, Journal of Catalysis 253 (2008) 37–49.
[28] W. Yao, R. Wang, X. Yang, Catalysis Letters 130 (2009) 613–621.
[29] A. Eyssler, P. Mandaliev, A. Winkler, P. Hug, O. Safonova, R. Figi, A. Weidenkaff, D. Ferri, Journal of Physical Chemistry C 114 (2010) 4584–4594.
[30] H. Tanaka, I. Tan, M. Uenishi, M. Kimura, K. Dohmae, Topics in Catalysis 1617 (2001) 63–70.
[31] U. Singh, J. Li, J. Bennett, A. Rappe, R. Seshadri, S. Scott, Journal of Catalysis 249 (2007) 349–358.
[32] S.J. Kim, S. Lemaux, G. Demazeau, J.Y. Kim, J.H. Choy, Journal of Materials Chemistry 12 (2002) 995–1000.
[33] M. Uenishi, M. Taniguchi, H. Tanaka, M. Kimura, Y. Nishihata, J. Mizuki, T. Kobayashi, Applied Catalysis B 57 (2005) 267–273.
[34] Y. Nishihata, J. Mizuki, H. Tanaka, M. Uenishi, M. Kimura, Journal of Physics and Chemistry of Solids 66 (2005) 274–282.
[35] A. Eyssler, E. Kleymenov, A. Kupferschmid, M. Nachtegaal, M.S. Kumar, P. Hug, A. Weidenkaff, D. Ferri, Journal of Physical Chemistry C 115 (2011) 1231–1239.
[36] S. Sartipi, A.A. Khodadadi, Y. Mortazavi, Applied Catalysis B 83 (2008) 214–220.
[37] J.M. Giraudon, A. Elhachimi, F. Wyrwalski, S. Siffert, A. Aboukaïs, J.F. Lamonier, G. Leclercq, Applied Catalysis B 75 (2007) 157–166.
[38] R. Lago, G. Bini, M.A. Pena, J.L.G. Fierro, Journal of Catalysis 167 (1997) 198–209.
[39] M. Engelmann-Pirez, P. Granger, G. Leclercq, Catalysis Today 107–108 (2005) 315–322.
[40] W.J. Shen, M. Okumura, Y. Matsumura, M. Haruta, Applied Catalysis A 213 (2001) 225–232.
[41] J. Liu, Z. Zhao, C.M. Xu, A.J. Duan, Applied Catalysis B 78 (2008) 61–72.
[42] J. Liu, Z. Zhao, C.M. Xu, A.J. Duan, G.Y. Jiang, Journal of Physical Chemistry C 112 (2008) 5930–5941.
[43] S. Liu, A. Obuchi, J. Oi-Uchisawa, T. Nanba, S. Kushiyama, Applied Catalysis B 37 (2002) 309–319.
[44] Q. Li, M. Meng, N. Tsubaki, X.G. Li, Z.Q. Li, Y.N. Xie, T.D. Hu, J. Zhang, Applied Catalysis B 91 (2009) 406–415.